Lilly Mercy et al. 2018. *Int. J. Vehicle Structures & Systems*, 10(6), 458-466
ISSN: 0975-3060 (Print), 0975-3540 (Online)
doi: 10.4273/ijvss.10.6.15

International Journal of Vehicle Structures & Systems
Available online at www.maftree.org/eja

Finite Element Modelling and Analysis of Micro-Capsule Based Self-Healing Polymeric Composites

J. Lilly Mercy[a] and S. Prakash

School of Mech. Engg., Sathyabama Institute of Sci. and Tech., Tamil Nadu, India
[a]Corresponding Author, Email: lillymercy.j@gmail.com

ABSTRACT:

Self-healing polymeric composites are a class of functional composites which heal itself during damage. Out of the many methods of self-healing, micro-capsule based self-healing process is the proven and established method where the healing agent stored in the capsule breaks and seals up the gap after the polymerization reaction with the suitable catalyst. The incorporation of the capsule in a polymer matrix in a random fashion makes it challenging to model the composite material. This paper explains the modelling and simulation of the self-healing composite using MIDAS NFX FEA software. The effect of self-healing composition - micro-capsule size and concentration on the static mechanical properties of the composite is explored. The capsules are integrated in the polymer matrix as a representative volume element using the rule of mixtures. The classical laminate theory was used to identify the critical ply failure.

KEYWORDS:

Self-healing; Finite element modelling; Micro-capsule; Classical laminate analysis; MIDAS NFX

CITATION:

J. Lilly Mercy and S. Prakash. 2018. Finite Element Modelling and Analysis of Micro-Capsule Based Self-Healing Polymeric Composites, *Int. J. Vehicle Structures & Systems*, 10(6), 458-466. doi:10.4273/ijvss.10.6.15.

1. Introduction

Simulating a sample with real life testing conditions is useful to predict the nature of a material. Several modelling and analysis studies have been done on fibre reinforced composites. Simulation of crack growth for bamboo fibre reinforced epoxy composites were investigated by Linear Elastic Fracture Mechanics (LEFM) approach using ABAQUS [1]. Three dimensional progressive failure models were done by Do-Hyoung et al [2] for GFRP composite to predict the non-linear mechanical response under impact load. The commercial software LS-Dyna was used for the modelling process. The properties of the individual elements in a fibre reinforced composite can be consolidated and approximated to a single property of the composite to perform finite element analysis using ANSYS workbench as discussed by Deshmukh and Jaju [3], Vishnu et al [4]. However, there was a vast difference in the behaviour of the material in real time when loading is done along a particular direction. The orthotropic nature of the fibre reinforced composite was translated to the isotropic property which lead to redundant results.

Layered finite element modelling was found to be highly dependable in case of laminated composites [5]. A combination of linear analysis and delamination model using ANSYS was proposed by Zhang [6]. The mathematical equations in the Classical Laminate Theory (CLT) were used to define the stress and strain across different directions. The first ply failure criterion was used to determine the strength of the layered composite. ANSYS works on Tsai Wu failure criterion, and hence that was employed to measure the first ply failure. In this paper, finite element modelling and simulation of micro-capsule based self-healing polymer composites is discussed. The micro-capsule is modelled using a representative volume element (RVE) based approach. The finite element analysis (FEA) is carried out before hand to predict the mechanical test loads and also study the sensitivity of various concentrations and sizes of the micro-capsule on the simulated mechanical test models. All the simulations are performed as a linear static solution using MIDAS NFX FEA software.

2. Boundary conditions validation

In FEA, the idealisation of real test conditions in most representative yet accurate way becomes an important aspect to rely on the outcome of simulation [7]. Table 1 lists the mechanical tests to be simulated along with their ASTM specifications and specimen dimensions. For simplicity and validation of boundary conditions for each mechanical test, the isotropic properties [8] of cured neat Epoxy LY556 resin mixed with HY951 hardener in the ratio of 10:1, as given in Table 2 are used. The neat resin FE models are idealised using CHEXA type solid element. The loading and boundary conditions are applied using RIGID BODY type element with its MASTER node being dependent on all the degrees of freedom (DOF). For all the mechanical tests, the refinement of FE mesh is maintained such that the element length along the length and width of specimen as 1mm and through the thickness as 0.5mm as shown in Fig. 1. For the tensile and flexure test specimen models, further refinement of the mesh at the mid-width and mid-span is carried as shown in Fig. 2. Details of the mid-

span mesh refinement for the in-plane strength test specimen is shown in Fig. 3. In Fig. 3, the double notches of 1mm width and 1.5mm deep are 6.5mm apart. A summary of the neat resin FE model for all the test specimens are given in Table 3.

Table 1: Mechanical test specifications and specimen dimensions

Test	ASTM standard	Specimen dimensions (mm)	Additional details
Tensile strength	D3039	250×25×3	Clamping tab length is 56mm
Compressive Strength	D695	15×15×3	Anti-buckling guide is enabled
Flexure strength	D790	120×13×3	Support rollers span is 50mm
In-plane shear strength	D3846	200×25×3	Tensile loading

Table 2: Mechanical properties of cured neat Epoxy LY556/HY951

Property	Value	Unit
Density	1200-1250	kg/m^3
Poisson ratio	0.35	-
Tensile modulus	3.1-3.3	GPa
Tensile strength	83-93	MPa
Elongation	4.2-5.6	%
Flexure strength	115-125	MPa

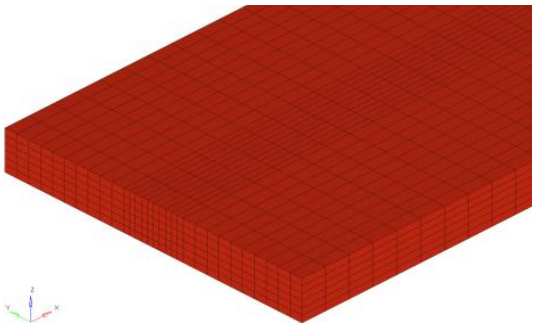

Fig. 1: FE mesh refinement at edge of the specimen

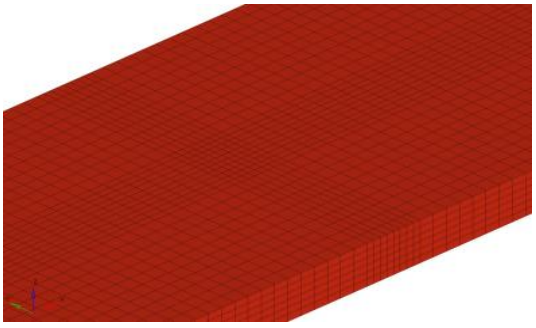

Fig. 2: FE mesh refinement at mid-span the specimen

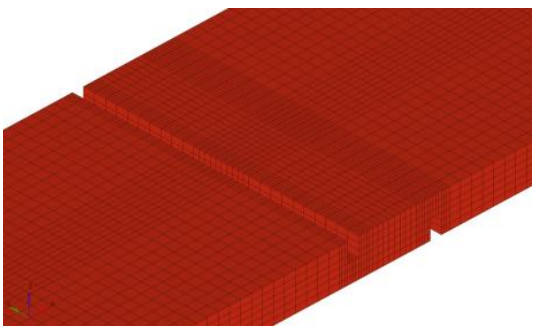

Fig. 3: FE mesh refinement at mid-span the In-plane shear test

Table 3: FE model summary (neat resin)

Test	Model ID	CHEXA elements	RIGID elements	Nodes
Tensile strength	M1-00	35,640	2	43,185
Compressive Strength	M2-00	2,407	1	3,088
Flexure strength	M3-00	13,392	1	16,626
In-plane shear strength	M4-00	29,160	2	35,683

The FE mesh of the tensile test specimen with neat resin material properties is shown in Fig. 4. The master node of left hand side RIGID element is constrained in all DOF to simulate a clamped boundary condition. A uni-axial tensile load of 25 kN in X-direction is applied at the master node of right hand side RIGID element. The fringe plots of displacement and mid-span stress tensor in the X-direction from the linear static analysis are presented in Fig. 5 and Fig. 6 respectively. The analytical solutions for the displacement and stress are calculated using,

$$\delta = \frac{F\,L}{E_r\,b\,t} \tag{1}$$

$$\sigma = \frac{F}{b\,t} \tag{2}$$

Where F is applied force, L is the distance between the clamps, E_r is the elastic modulus of neat resin = 3,300 MPa, b and t are width and thickness of the specimen.

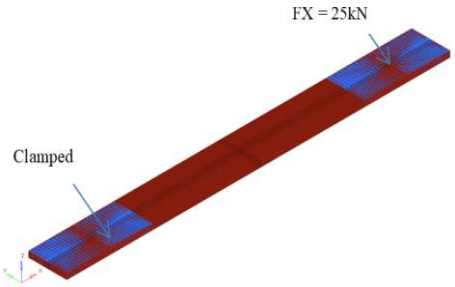

Fig. 4: FE mesh for tensile test validation model

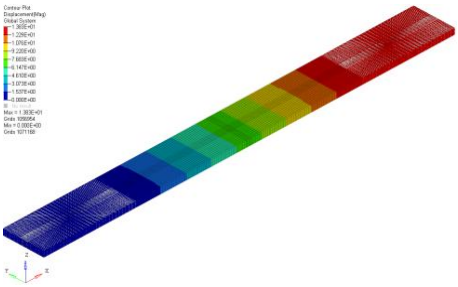

Fig. 5: Displacement fringe for tensile test validation model

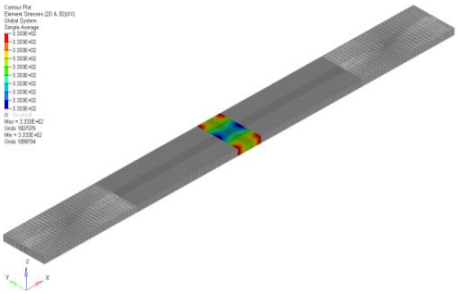

Fig. 6: Stress fringe for tensile test validation model

The FE mesh of the compressive test specimen with neat resin material properties is shown in Fig. 7. All the nodes at left hand face are constrained in all DOF to simulate a clamped boundary condition. The nodes at the top/bottom faces and front/back faces are respectively constrained as TZ = 0 and TY = 0 to simulate a pure compression. A uni-axial compressive load of 65 kN in X-direction is applied at the master node of right hand side RIGID element. The fringe plots of displacement and stress tensor in the X-direction from the linear static analysis are presented in Fig. 8 and Fig. 9 respectively. The displacement is analytically calculated by taking into account of the stresses due to the compression induced Poisson ratio effect in the other directions using,

$$\delta = \frac{F\,l}{E_r\,b\,t}\left(1 - \frac{2\mu_r^2}{1-\mu_r}\right) \quad (3)$$

Where l is the length of the specimen and μ_r is the Poisson ratio of the neat resin = 0.35. The compressive stress can be calculated using Eqn. (2).

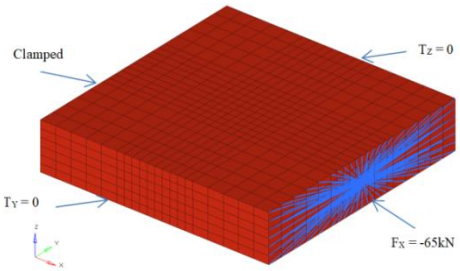

Fig. 7: FE mesh for compressive test validation model

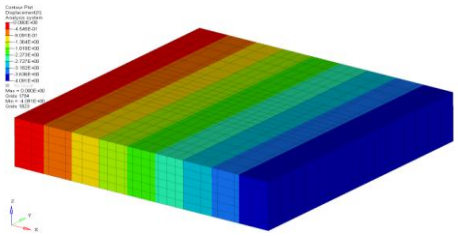

Fig. 8: Displacement fringe for compressive test validation model

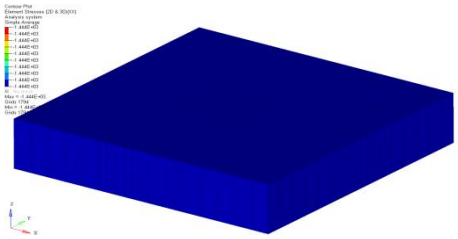

Fig. 9: Stress fringe for compressive test validation model

The FE mesh of the three point bending (flexure) test specimen with neat resin material properties is shown in Fig. 10. The nodes on the specimen in contact with support rollers (span = 50mm) are constrained as TZ = 0 to idealize a simply supported boundary condition. The nodes on the specimen in contact with loading roller are constrained as TX = 0 to idealize no-slip during loading state. A vertical load of 3.5 kN in Z-direction is applied at the master node of loading roller RIGID element. In order to accurately extract the extreme fiber stresses during flexure, 2D SHELL elements with elastic modulus being the same as that of neat resin (3.3 GPa) are introduced with negligible thickness of 0.001mm. The fringe plots of displacement in Z-direction and stress tensor in the X-direction from the linear static analysis are presented in Fig. 11 and Fig. 12 respectively. These displacement and flexural stress results are validated through hand calculations using,

$$\delta = \frac{F\,d^3}{4\,E_r\,b\,t^3} \quad (4)$$

$$\sigma = \frac{3\,F\,d}{2\,b\,t^2} \quad (5)$$

Where d is the distance between support rollers = 50mm.

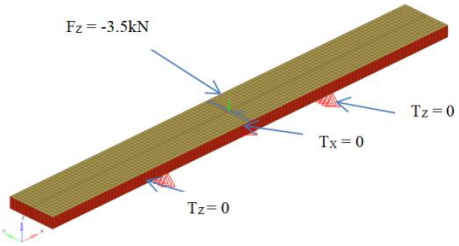

Fig. 10: FE mesh for flexure test validation model

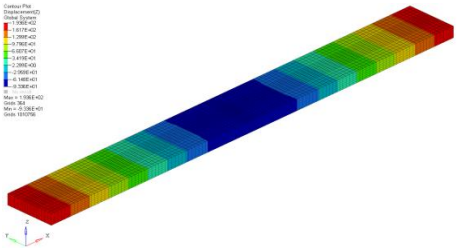

Fig. 11: Displacement fringe for flexure test validation model

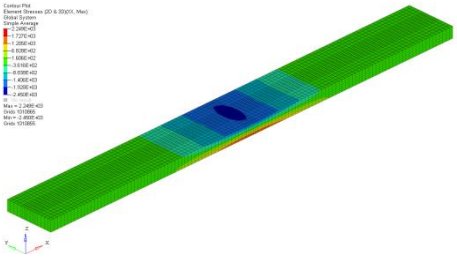

Fig. 12: Stress fringe for flexure test validation model

The FE mesh of the Double Notch Shear (DNS) test specimen with neat resin material properties for in-plane shear strength determination is shown in Fig. 13. The master node of left hand side RIGID element is constrained in all DOF to simulate a clamped boundary condition. A uni-axial tensile load of 15 kN in X-direction is applied at the master node of right hand side RIGID element. Due to double notches, the top and bottom surface nodes are constrained as TZ = 0 to restrain the out-of-plane bending, thereby simulate a pure in-plane shear load transfer at the mid-thickness of the specimen when the tensile load is applied at the right end. The fringe plots of displacement in X-direction, maximum shear stresses at mid-span from the linear static analysis are presented in Fig. 14 and Fig. 15 respectively. These displacement and flexural stress results are validated through hand calculations using,

$$\delta = \frac{F}{E_r\,b}\left(\frac{\mathrm{L}-2\mathrm{f}}{\mathrm{t}} + \frac{2\,\mathrm{f}}{\mathrm{t}-\mathrm{e}}\right) \quad (6)$$

$$\sigma = \mathrm{F}/(\mathrm{c\ b}) \quad (7)$$

Where e and f are the depth (1.5mm) and width (1mm) of the notch respectively. c is the distance (6.5mm) between the double notches.

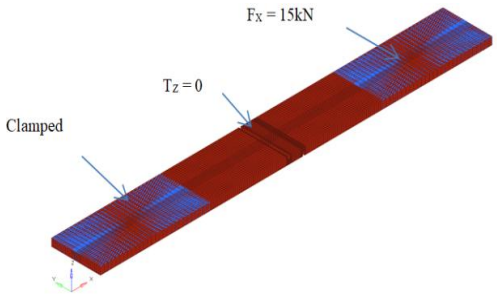

Fig. 13: FE mesh for DNS test validation model

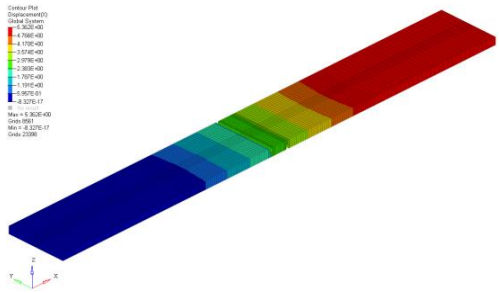

Fig. 14: Displacement fringe for DNS test validation model

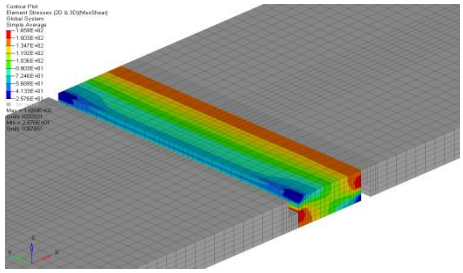

Fig. 15: Fringe of max. shear stress at mid-span for DNS test validation model

Table 4 gives a summary of the FEA results in comparison with the analytical calculations using Eqns. (1) to (7) for the validation of the boundary conditions to simulate the tensile, compressive, flexural and in-plane shear strength tests. Tensile and compressive loaded model results matched 100% with the analytical solutions. The FEA displacement from flexural test simulation model is 1.1% lesser than the calculation. Likewise, the flexure stress at mid-span from FEA is 1% higher than the analytical calculation. Given the fact that the three point bending test involves a contact friction between the rollers and the specimen, the flexure test validation model results are deemed as acceptable. The displacement in X-direction from FEA of DNS test is 1.1% higher than the analytical solution. The deviation of FEA stress result of DNS test simulation from calculation is 3.8%. The extraction of in-plane shear stress at the mid-plane is relied upon the averaging of its adjacent SOLID elements. Hence, the predicted results for the in-plane shear strength test validation model are deemed as acceptable.

Table 4: Neat resin FEA results: Boundary conditions validation

Model ID	FEA δ (mm)	Analytical δ (mm)	FEA σ (MPa)	Analytical σ (MPa)
M1-00	13.83	13.83	333.3	333.3
M2-00	4.09	4.09	1444.4	1444.4
M3-00	93.4	94.4	2249.0	2243.6
M4-00	5.36	5.30	95.8	92.3

3. FEA of GFRP without micro-capsule

The fabricated mechanical test specimens had 5 layers of plain weave E-Glass fabric (300 gsm) with the orientations of {0/90}/±45/{30/60}/±45/{0/90}. The glass fabric is idealized using 2D SHELL CQUAD4 elements with a thickness of 0.2mm. The neat resin based validated FE models have been amended to include these SHELL elements at every 0.5mm thickness for each layer as shown in Fig. 16. The woven fabric material orientations such as ±45, 0/90 and 30/60 are accounted by defining a PCOMP material card as available in the MIDAS NFX FEA software for defining composite materials. The SHELL mesh of each reinforcement layer is shown in Fig. 17. The 0° orientation is aligned to the X-axis of global coordinate system. The mechanical properties of the 0/90 woven E-Glass fabric reinforced (50% fiber volume fraction) epoxy layer are given in Table 5. These values were taken from Hexcel Prepreg Tech. Handbook [9].

Table 5: Properties of 0/90 woven E-Glass fabric reinforced Epoxy

Property	Value	Strength property	Value (MPa)
$E_{\parallel}$	20 GPa	X_t	600
$E_{\perp}$	19 GPa	X_c	550
$\gamma_{\parallel\perp}$	0.130	Y_t	550
$G_{\parallel\perp}$	4200	Y_c	550
ρ	2.2 g/cc	SC	55

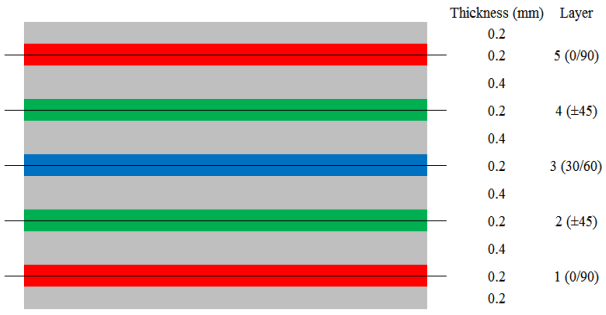

Fig. 16: Modelling details of woven E-Glass and resin layers

As the FE simulation of mechanical test represents the cured woven fabric behaviour, it is acceptable to use these values for modelling with a small correction to the thickness to discount the resin impregnation. As seen in Fig. 16, the thickness of modelled resin element is 0.5mm per layer. However, to avoid double accounting of the reinforcement layer thickness being 0.2mm, the elastic modulus of resin (E_{rr}) layer was corrected as follows,

E_{ro} for base and top resin layers = 3300 * 0.2/0.5
= 1320 MPa

E_{ri} of intermediary resin layers = 3300 * 0.4/0.5
= 2640 MPa

All the validated mechanical test FE models were re-run with same set of loads and boundary conditions after incorporating the woven E-Glass reinforcement layers' SHELL CQUAD4 elements and resin layers' BRICK CHEXA elements with corrected elastic modulus. The obtained results from the FE simulations of all 4 tests are presented in Fig. 18 to Fig. 21. A summary of FEA simulation results are given in Table 6.

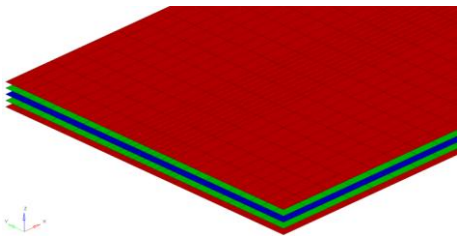

Fig. 17: FE mesh of reinforcement layers (resin mesh not shown)

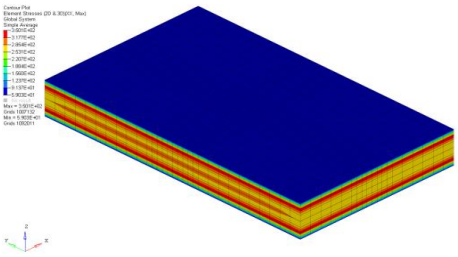

Fig. 18: GFRP – Tensile stress at mid-span

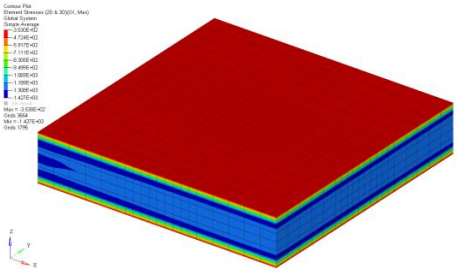

Fig. 19: GFRP - Compression stress at mid-span

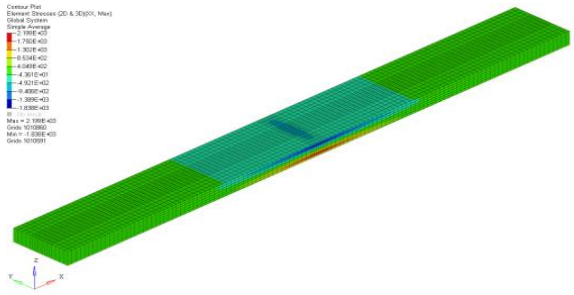

Fig. 20: GFRP – flexure stress at mid-span

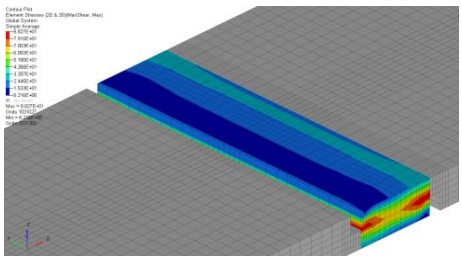

Fig. 21: GFRP – In-plane shear stress at mid-span

Table 6: GFRP without micro-capsule FEA results summary

Model ID	Load (kN)	Displacement (mm)	Stress (MPa)
M1-01	25	6.04	350.1
M2-01	65	2.38	1427
M3-01	3.5	54.28	2199
M4-01	15	2.5	56.4

In order to validate the FEA results for the GFRP specimens without micro-capsule, classical laminate analysis (CLA) has been carried out to identify the critical ply, interface region and associated failure type, i.e. fibre or matrix for the tensile, compressive and flexure test. For in-plane shear test, the critical interface is the one at the mid-plane, i.e. {30/60} ply. CLA is carried out using eLamX software from Technische Universität, Dresden. Each ply with resin interface was idealised as a single layer with cured ply thickness of 0.6mm and maximum stress failure criterion has been chosen for CLA. For tensile, compressive and flexure test, the loading parameters within the eLamX software were set as, n_x = 100 N/mm, n_x = -100 N/mm and m_x = 100 N/mm respectively. The CLA results for tensile, compressive and flexure test were presented in Fig. 22 to Fig. 24 respectively. From the results, it is very clear that the critical ply interface for all these failures is between the {0/90} and ±45 layers dominated by a matrix failure. The peak stress locations on the stress fringe plots from FEA (see Fig. 18 to Fig. 21) were matched well to the CLA results. Thus, the FEA simulations for GFRP specimens without capsules are validated.

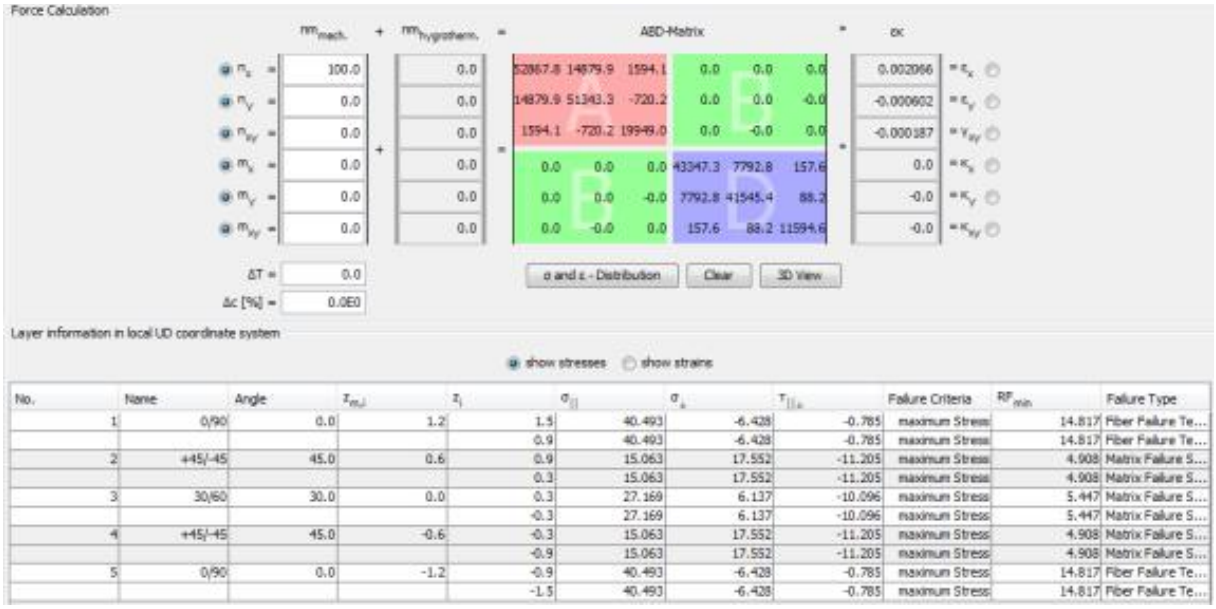

No.	Name	Angle						Failure Criteria		Failure Type
1	0/90	0.0	1.2	1.5	40.493	-6.428	-0.785	maximum Stress	14.817	Fiber Failure Te...
				0.9	40.493	-6.428	-0.785	maximum Stress	14.817	Fiber Failure Te...
2	+45/-45	45.0	0.6	0.9	15.063	17.552	-11.205	maximum Stress	4.908	Matrix Failure S...
				0.3	15.063	17.552	-11.205	maximum Stress	4.908	Matrix Failure S...
3	30/60	30.0	0.0	0.3	27.169	6.137	-10.096	maximum Stress	5.447	Matrix Failure S...
				-0.3	27.169	6.137	-10.096	maximum Stress	5.447	Matrix Failure S...
4	+45/-45	45.0	-0.6	-0.3	15.063	17.552	-11.205	maximum Stress	4.908	Matrix Failure S...
				-0.9	15.063	17.552	-11.205	maximum Stress	4.908	Matrix Failure S...
5	0/90	0.0	-1.2	-0.9	40.493	-6.428	-0.785	maximum Stress	14.817	Fiber Failure Te...
				-1.5	40.493	-6.428	-0.785	maximum Stress	14.817	Fiber Failure Te...

Fig. 22: CLA results for tensile loading

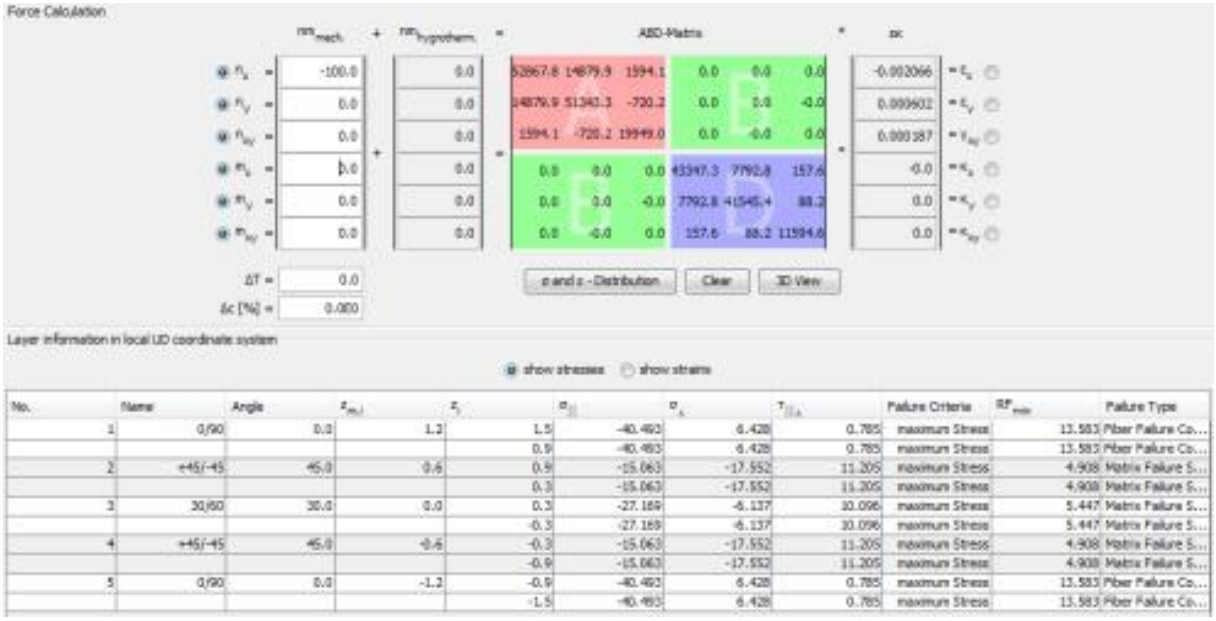

Fig. 23: CLA results for compressive loading

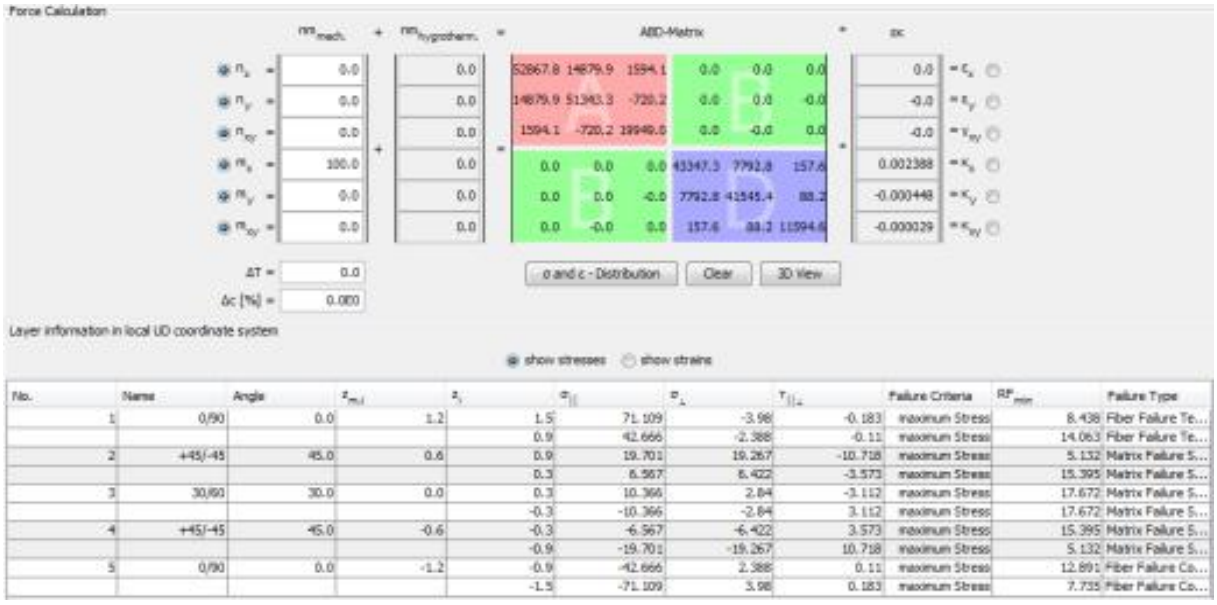

Fig. 24: CLA results for flexure loading

4. FEA of GFRP with micro-capsule

The self-healing composites are heterogeneous in nature, made up of materials with different physical and mechanical properties. Micromechanics help to narrow down the heterogeneous properties of the composite to homogenised properties. This can be achieved through defining a Representative Volume Element (RVE). Self-healing GFRP contains micro-capsules, catalyst, glass fibres, epoxy resin etc. All these ingredients could be defined in a smaller 3-dimensional shaped RVE to arrive the properties of the whole material. RVE of epoxy resin and micro-capsules were created using simple cube architecture and mirrored pyramid architecture within a block of 0.5×0.5×0.5mm FE volume as shown in Fig. 25. The spherical micro-capsule was modelled as a unit cell of poly(urea-formaldehyde) using 2DSHELL elements of CTRIA3 type for pyramid RVE and CQUAD4 type for cube RVE respectively.

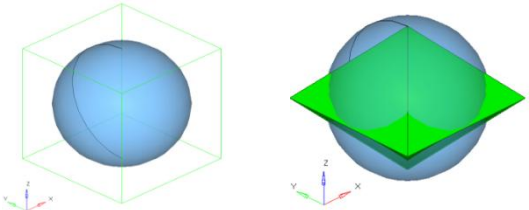

Fig. 25: FE model of micro-capsule using cube RVE (left) and mirrored pyramid RVE (right)

Irrespective of the size of the micro-capsule, the elastic modulus and Poisson ratio for a 0.2μm thickness shell wall of a single micro-capsule was found to be 3.7GPa and 0.33 respectively [10]. Then this micro-capsule RVE was integrated into the reinforced epoxy resin element volume. The evolution of meshing for the mirrored pyramid RVE is shown in Fig. 26. The element quality checks were performed using MIDAS NFX FEA software and found that the mesh quality was met the FEA standard practices. The FE models for the micro-

capsule integrated into resin element for the cube and pyramid RVEs are shown in Fig. 27. The number of nodes and elements used is summarised in Table 7. For tensile, compressive and flexure test specimens, these RVEs are integrated within the resin SOLID element between GFRP layers 1-2 and 4-5. For the DNS test model, these RVEs are integrated within the resin SOLID element between GFRP layers 2-3 and 3-4.

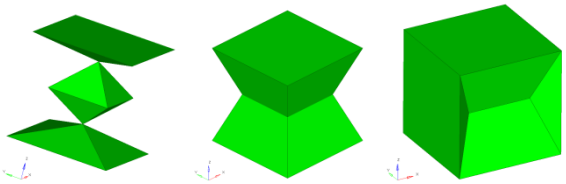

Fig. 26: Pyramid RVE mesh for micro-capsule within epoxy resin

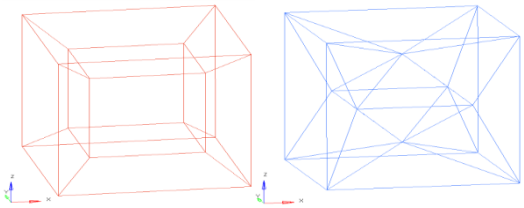

Fig. 27: FE models of cube RVE (Left) and mirrored pyramid RVE (Right) within epoxy resin

Table 7: RVE model summary

Details	Cube RVE	Pyramid RVE
TRIAs	N/A	8
QUADs	6	N/A
PYRAMIDs	N/A	10
PENTAs	N/A	4
HEXAs	6	N/A
NODES	16	14

The concentration of micro-capsule dispersed into the neat epoxy resin is modelled using "Lattice Structure" architecture. For the lattice structure, the refined mesh at the mid-width region of 2mm×5mm at the mid-span has been chosen. This represents 4 elements along the span and 10 elements across the width, amounting total of 40 elements with each element volume being 0.5×0.5×0.5mm. As the dispersion of micro-capsules is very random and uncontrolled, a random number of elements that is equivalent to the percentage concentration of micro-capsule with in lattice structure were replaced with cube and pyramid RVEs at appropriate interfaces. For the 40 elements lattice structure as shown in Fig. 28, the proportionate RVEs for 5%, 15% and 25% micro-capsule concentration into neat resin are 2, 6 and 10 respectively.

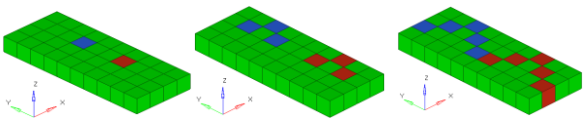

Fig. 28: Locations of RVE (red - cube, blue - pyramid) within the epoxy resin lattice structure for micro-capsule concentrations - 5% (left), 15% (middle) and 25% (right)

The finite elements away from the lattice structure are idealised using isotropic material properties accounting the percentage concentration of micro-capsule dispersions into the near epoxy matrix using rule of mixtures. The elastic modulus (E_{cr})and Poisson ratio (μ_{cr}) of the epoxy resin mixed with the capsules are calculated using the rule of mixtures by knowing the volume concentration of the micro-capsule as follows,

$$E_{cr} = E_c * V_c + E_r * V_r \quad (8)$$

$$\mu_{cr} = \mu_c * V_c + \mu_r * V_r \quad (9)$$

Where V_c and V_r are the volume fraction (i.e. % concentration) of micro-capsule and neat resin respectively. Table 8 gives the calculated elastic modulus and Poisson ratio. The resin properties were further corrected to account for the difference between idealised resin thickness on the FE model and to avoid double accounting of the thickness contribution from the GFRP SHELL element layer. The models for the 5%, 15% and 25% concentrations of micro-capsule were identified by M*05, M*15 and M*25 respectively. The * is replaced with 1, 2, 3 and 4 for tensile, compressive, flexure and DNS test simulation models.

Table 8: Modulus and Poisson ratio of epoxy resin with various micro-capsule concentrations

Property	Actual	Top & base resin layers, FEM	Intermediary resin layers, FEM
E_{cr} 5% (MPa)	3320	1328	2656
E_{cr} 15% (MPa)	3360	1344	2688
E_{cr} 25% (MPa)	3400	1360	2720
μ_{cr} 5%		0.349	
μ_{cr} 15%		0.347	
μ_{cr} 25%		0.345	

The FE models for GFRP integrated with micro-capsule RVE models were solved using linear static analysis for same set of boundary conditions and loading as undertaken for the validation models. For each FEA, the maximum displacement, peak stress tensor and von mises stress within the micro-capsule element were assessed. The displacement and stress fringe plots for 5%, 15% and 25% concentrations of micro-capsules were assessed in detail. The displacement of GFRP specimens with micro-capsule was of similar magnitude to those of GFRP specimens alone. Also, the stress distribution at the mid-span was almost similar for all the concentrations of the micro-capsule. Hence, the stress fringe plot for the 25% concentration of micro-capsule was only presented for each test simulation, in Figs. 29, 31, 33 and 35. The von mises stress for the micro-capsule wall and a cross-section view of micro-capsule interaction with the epoxy resin for all the concentrations analyzed were presented in Figs. 30, 32, 34 and 36. The percentage increase in micro-capsule concentration has consistently shown an improvement in the peak stress observed in the self-healing composite specimen test FEA simulations.

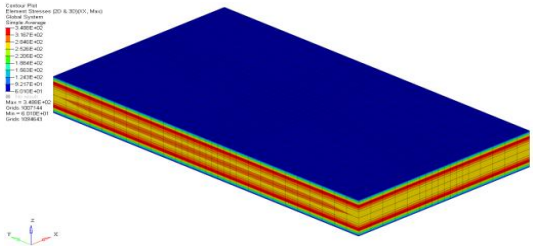

Fig. 29: GFRP with 25% micro-capsule – tensile stress at mid-span

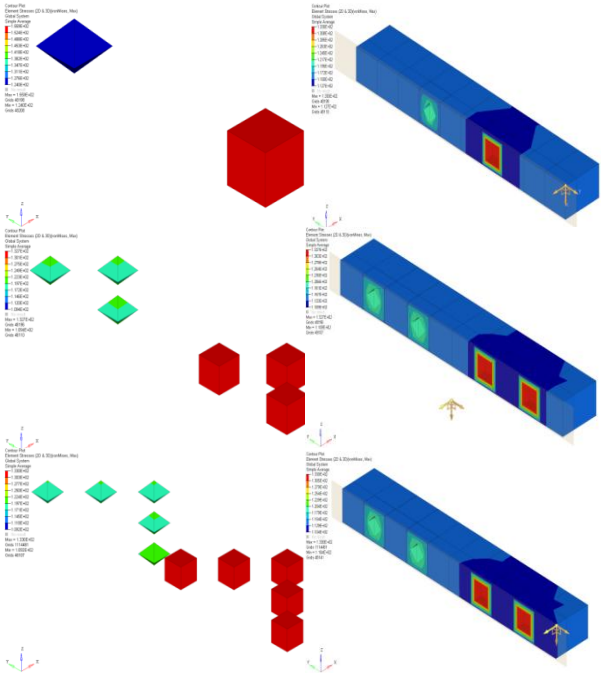

Fig. 30: Tensile test of GFRP with micro-capsule - von mises stress (left) and interaction with epoxy resin (right) for various concentrations, 5% (top), 15% (middle) and 25% (bottom)

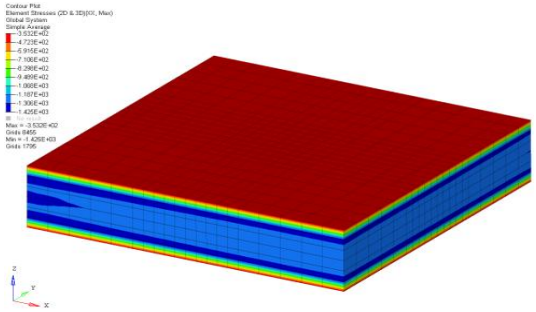

Fig. 31: GFRP with 25% micro-capsule – Comp. stress at mid-span

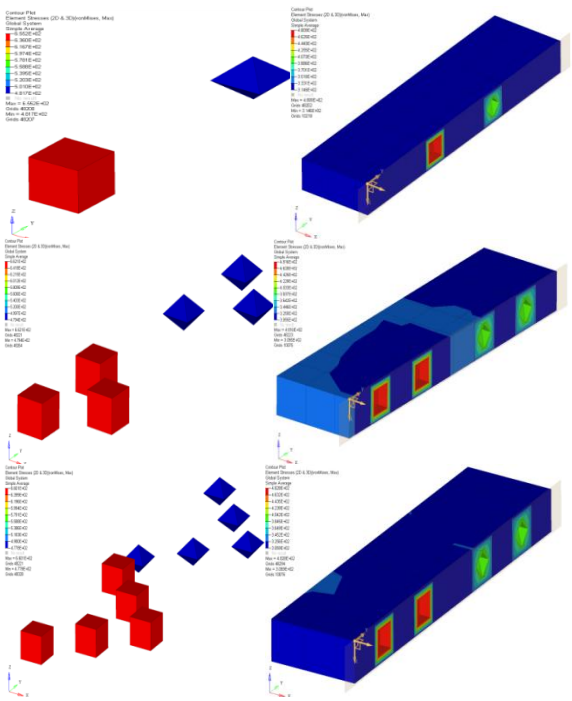

Fig. 32: Compression test of GFRP with micro-capsule - von mises stress (left) and interaction with epoxy resin (right) for various concentrations, 5% (top), 15% (middle) and 25% (bottom)

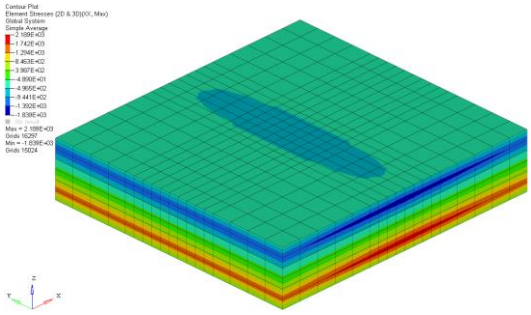

Fig. 33: GFRP with 25% micro-capsule - Flexure stress at mid-span

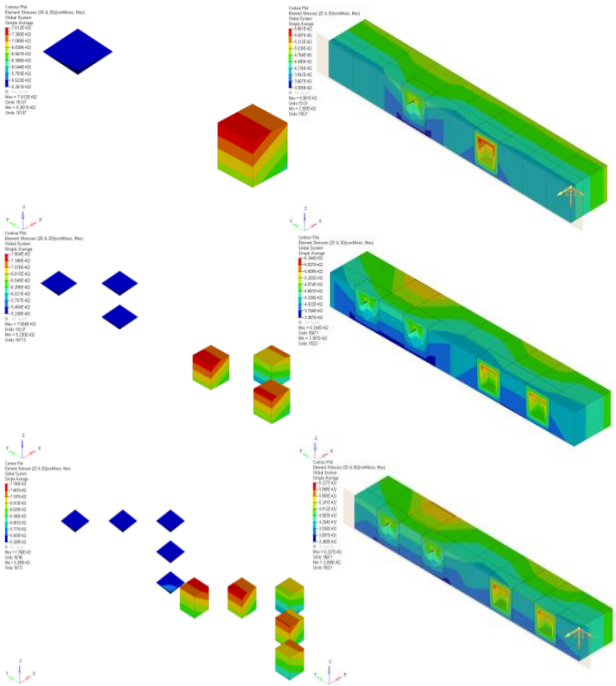

Fig. 34: Flexure test of GFRP with micro-capsule - von mises stress (left) and interaction with epoxy resin (right) for various concentrations, 5% (top), 15% (middle) and 25% (bottom)

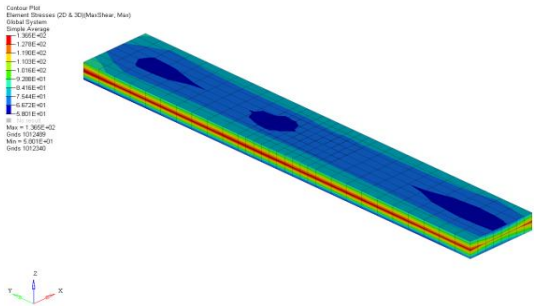

Fig. 35: GFRP with 25% micro-capsule – In-plane shear stress at mid-span and mid-thickness

The cube RVE has shown higher von mises stress values than the Pyramid RVE, demonstrating that it is stiffer than the detailed mirrored pyramid RVE model for the micro-capsule. However, for the flexure test and in-plane shear test simulations, the pyramid RVE has shown good interaction with the epoxy resin. Thus, the pyramid RVE model is preferred for any further detailed simulations. Table 9 summarises the FEA results for GFRP specimens with micro-capsule. It should be noted that the applied loads to the FEA simulations are relatively higher than the possible failure load in the experimental test. The varied percentage concentrations

of micro-capsule to the GFRP test specimens has shown consistent improvements in all four tested strengths, in particular for flexural and in-plane shear strengths, the micro-capsule concentration has shown a better interaction with the epoxy resin.

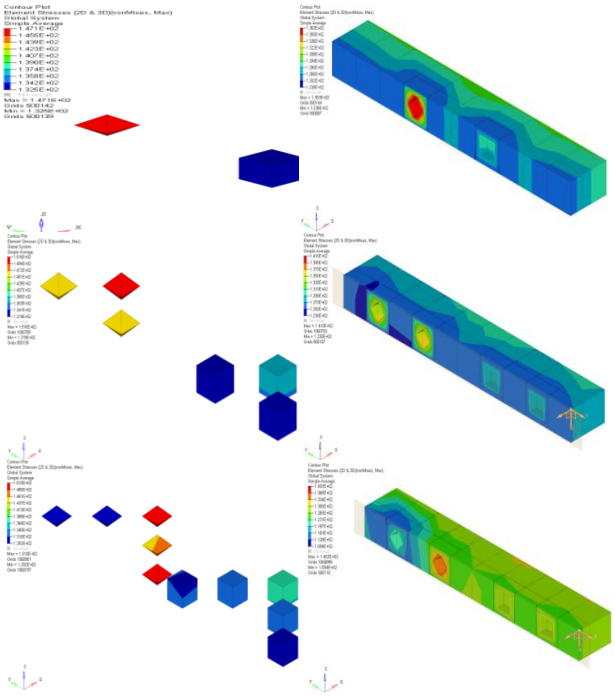

Fig. 36: In-plane shear test of GFRP with micro-capsule - von mises stress (left) and interaction with epoxy resin (right) for various concentrations, 5% (top), 15% (middle) and 25% (bottom)

Table 9: GFRP with micro-capsule - FEA results summary

Model ID (% micro-capsule)	Peak stress, composite (MPa)	Peak von mises stress, micro-capsule (MPa)
M1-05 (5%)	349.8	155.9
M1-15 (15%)	349.3	132.7
M1-25 (25%)	348.8	133.0
M2-05 (5%)	1427	655.2
M2-15 (15%)	1426	662.1
M2-25 (25%)	1425	660.1
M3-05 (5%)	2197	761.2
M3-15 (15%)	2193	760.4
M3-25 (25%)	2189	776.6
M4-05 (5%)	92.8	147.1
M4-15 (15%)	88.5	151.6
M4-25 (25%)	88.5	151.0

5. Conclusion

The FEA simulation of self-healing GFRP composite using RVE model has been performed using MIDAS NFX FEA software. In order to trust the FEA predictions, the loading and boundary conditions were established for tensile, compressive, flexural and in-plane shear test through the use of neat cured epoxy resin isotropic properties. Validation of post-processed displacement and maximum stresses with analytical calculations proved the simulated boundary conditions are acceptable.The GFRP without micro-capsule test models and their predicted peak stress locations were verified through CLA using eLamX. These results were also assessed to choose the resin layer to integrate the micro-capsule RVE models. The micro-capsule RVE models were idealized as a simple cube shape as well as a mirrored pyramid shape to establish the accurate modelling of micro-capsule interaction within the epoxy resin. The FEA results have shown that the pyramid RVE better simulates the micro-capsule behavior than the cube due to the fact that simplified cube RVE model being stiffer. The dispersion of micro-capsules into the epoxy resin has been idealized using a lattice structure concept for 5%, 15% and 25% concentration of micro-capsules. The sensitivity of the percentage concentration of micro-capsules has shown a consistent improvement.

REFERENCES:

[1] Z. Khan, B.F. Yousif and M. Islam. 2017. Fracture behaviour of bamboo fibre reinforced epoxy composites, *Composites Part B: Engg.*, 116, 186-199. https://doi.org/10.1016/j.compositesb.2017.02.015.

[2] D.H. Kim, K.H. Jung, I.G. Lee, H.J. Kim and H.S. Kim. 2017. Three dimensional progressives failure modelling of glass fibre reinforced thermoplastic composites for impact simulation, *Composite Structures*, 176(15), 757-767. https://doi.org/10.1016/j.compstruct.2017.06.031.

[3] B.B. Deshmukh and S.B. Jaju. 2011. Design and analysis of glass fibre reinforced polymer leaf spring, *Proc. 4th Int. Conf. Emerging Trends in Engg & Tech.*, 82-87. https://doi.org/10.1109/ICETET.2011.61.

[4] V. Prasad, A. Joy, G. Venkatachalam, S. Narayanan and S. Rajakumar. 2014. Finite element analysis of Jute and Banana fibre reinforced hybrid polymer matrix composite and optimisation of design parameters using ANOVA technique, *Proc. Engg.*, 97, 1116-1125. https://doi.org/10.1016/j.proeng.2014.12.390.

[5] C.C. Lam. 2015. Finite element analysis of fibre reinforced polymer rehabilitation of cracked steel and application to pipe repair, *Rehabilitation of Pipelines using Fiber-reinforced Polymer Composites*, 135-175. https://doi.org/10.1016/B978-0-85709-684-5.00008-4.

[6] C. Zhang. 2010. *Finite Element Analysis of Glass Fibre Reinforced Polymer Bridge Decks*, MSc. Thesis, University of Manitoba.

[7] S.A. Hussain, B.S. Reddy and V.N Reddy. 2008. Prediction of elastic properties of FRP composite lamina for longitudinal loading, *ARPN J. Engg. and Applied Sciences*, 3(6), 70-75.

[8] *Hot curing epoxy system based on Araldite LY556/Hardener HY917/Accelerator DY 070, Data Sheet*, Publ. No.98010/e, February 1998, Ciba Specialty Chemicals, Switzerland.

[9] *Hexply Prepreg Tech.*, Publication No. FGU 017c, 2013, Hexcel Corporation (Solvay).

[10] M.W. Keller and N.R. Sottos. 2006. Mechanical properties of microcapsules used in a self-healing polymer, *Experimental Mechanics*, 46, 725-733. https://doi.org/10.1007/s11340-006-9659-3.